Finite Control Set Model-Free Predictive Current Control of PMSM With Two Voltage Vectors Based on Ultralocal Model

Zheng Sun, *Graduate Student Member, IEEE*, Yongting Deng, *Senior Member, IEEE*, Jianli Wang, *Member, IEEE*, Tian Yang, *Graduate Student Member, IEEE*, Zongen Wei, *Graduate Student Member, IEEE*, and Haiyang Cao, *Graduate Student Member, IEEE*

***Abstract*—Model-free predictive current control (MFPCC) that only needs the input and output data of the system can eliminate the influence of the motor parameters mismatch. In the conventional finite control set MFPCC (FCS-MFPCC), the delay and distortion that exist in the current variations update can affect the future current prediction and the current tracking performance. This article studies an improved current variations updating mechanism to improve the update frequency. Based on the ultralocal model, the current variations corresponding to the different voltage vectors can be updated at every control period. Then, the stator currents can be predicted with the accurate current variations, and the optimal voltage vector can be selected by minimizing the cost function without using motor parameters. Besides, a sliding mode observer is designed to observe the ultralocal model's parameters fast. Furthermore, the two voltage vectors and the optimal duration are introduced to improve the current tracking performance. Meanwhile, in order to guarantee the accuracy of the future current prediction, the current compensation strategy is studied to revise the current estimation. Finally, the effectiveness of the proposed FCS-MFPCC strategy is verified through the simulation and experimental results.**

***Index Terms*—Current variations updating, finite control set (FCS), model-free, permanent magnet synchronous motor (PMSM), predictive current control (PCC), ultralocal model.**

I. Introduction

DUE to the advantages of high power density, small size, good environmental adaptability, and excellent control performance, permanent magnet synchronous motor (PMSM) has been widely used in transportation, electrical, and other fields [1], [2], [3]. In order to achieve high-performance control, some control strategies, such as field-oriented control, direct torque control, and model predictive control (MPC), have been applied in the control system of PMSM. In recent years, MPC that has the advantages of predicting system behavior and improving control performance has received wide attention from scholars [4], [5], [6].

To improve the performance, current plays an important role in achieving fast response and stable torque. Some current control strategies, such as professional–integral–differential (PID) control, pulsewidth modulation (PWM) control [7], and predictive current control (PCC) [8], [9], [10], have also been studied in previous literature. However, compared with the PID and PWM control strategies, the PCC that can predict the future current of the system is able to achieve smaller steady-state error and better performance [11], [12]. According to different control variables, apart from PCC, predictive torque control [13], [14] and predictive speed control [15], [16] have also been studied by scholars.

In the previous literature, the finite control set model-based PCC (FCS-MBPCC) and its application in voltage source inverters are proposed in [17]. With the cost function, the switching state of the inverter is selected by predicting the currents corresponding to the different voltages. The advantage of this strategy is that it is simple and easy to implement by a digital signal processor (DSP). However, the system performance is affected by the parameters variation [18], [19], [20], and the influence is analyzed in [21] and [22]. The articles point out that, compared with the resistance mismatch, the influence of inductance mismatch is more serious to the current.

In order to solve the problem of parameters variation, some improved strategies that are based on the Kalman filter (KF) algorithm and the disturbance observer have been studied in [23] and [24]. In [23], an algorithm based on the KF is proposed to identify the parameters and reduce the current ripples caused by parameters variation. Similarly, a disturbance observer based on the stator current is proposed in [24]. Apart from the observer, the online identification strategies of the parameters are proposed in [25] and [26]. In [25], two offline projection algorithms that

Manuscript received 18 April 2022; revised 4 July 2022; accepted 10 August 2022. Date of publication 16 August 2022; date of current version 10 October 2022. This work was supported in part by the National Nature Science Foundation of China under Grant 11973041 and Grant 12122304 and in part by the Youth Innovation Promotion Association, Chinese Academy of Science under Grant 2019218. Recommended for publication by Associate Editor N. R. N. Idris. *(Corresponding authors: Yongting Deng; Jianli Wang.)*

Zheng Sun, Jianli Wang, Tian Yang, Zongen Wei, and Haiyang Cao are with the Department of Changchun Institute of Optics, Fine Mechanics, and Physics, Chinese Academy of Science, Changchun 130033, China, and also with the University of Chinese Academy of Sciences, Beijing 100049, China (e-mail: sunzheng19@mails.ucas.ac.cn; wangjianli@ciomp.ac.cn; yangtian19@mails.ucas.ac.cn; weizongen20@mails.ucas.ac.cn; caohaiyang20@mails.ucas.ac.cn).

Yongting Deng is with the Changchun Institute of Optics, Fine Mechanics, and Physics, Chinese Academy of Science, Changchun 130033, China (e-mail: dengyongting@ciomp.ac.cn).

Color versions of one or more figures in this article are available at https://doi.org/10.1109/TPEL.2022.3198990.

Digital Object Identifier 10.1109/TPEL.2022.3198990

are based on the discrete-time model of the PMSM are used to estimate the parameters. Besides, a new method that adds the feed-forward term to compensate for the current tracking error directly is proposed in [27]. Although the online identification strategy and the observer can estimate and compensate for the parameters mismatch, these methods increase the computational burden and introduce new parameters.

Apart from the methods aforementioned, FCS-MFPCC that can eliminate the influence of parameters mismatch has been proposed in [28] and [29]. Without using any parameters and the traditional SVPWM algorithm, the stator currents and their differences are applied to predict the future current in [28]. Meanwhile, the current differences caused by the different inverter switching states are stored in a lookup table (LUT). Therefore, according to the current differences in the table, the future current can be predicted to choose the optimal inverter switching state. However, the accuracy of the current prediction can be affected by the data update stagnant of the LUT because only one specific current difference can be updated in one cycle. In order to increase the update frequency of the LUT, an improved update strategy in [29] has been studied. The update frequency of the LUT is increased by applying a nonoptimal voltage vector to the inverter but that can increase the current ripples.

In order to solve the stagnation problem of the current gradient, a new current update strategy and prediction method are proposed in [30] and [31], respectively. In [30], the LUT of all voltage vectors can be updated in one control cycle. The current gradients caused by the voltage vectors of the previous two cycles are used to predict the future current gradient. Similarly, the previous two current time-derivatives (slope) are used to predict the future current in [31]. However, the divide operation will affect the convergence of the system when the adjacent voltages have small differences. Therefore, selecting the appropriate limiting value is necessary for this strategy. Apart from the MFPCC strategies based on the LUT, the MFPCC based on the ultralocal model is discussed in [32] and [33]. Different from [30] and [31], the MFPCC strategy in [32] and [33] is based on the continuous control set, and the reference voltage is predicted by using the ultralocal model.

In this article, in order to eliminate the delay and distortion that exist in the current variations update, an improved current variations updating mechanism that is based on the discrete-time ultralocal model is studied to improve the current variations updated frequency. Besides, a two-vector-based method is studied to decrease the current tracking error in the proposed FCS-MFPCC strategy. The main contributions of this study are summarized as follows:

1) An improved current variations updating mechanism that can increase the updated frequency is studied to eliminate the delay and distortion that exist in the current variations update.
2) To improve the current tracking performance of the proposed FCS-MFPCC strategy, the two-vector-based method is studied to synthesize the optimal voltage vector with the optimal duration that can be derived from the reference voltage vector and the cost function.

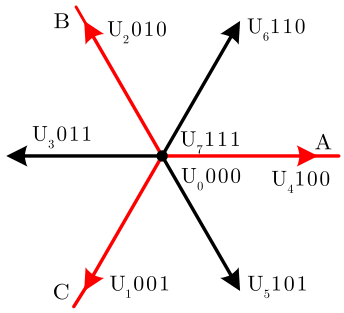

Fig. 1. Voltage vectors of the inverter.

3) A compensation strategy is studied to guarantee the accuracy of the current variations and the future current prediction because the two voltage vectors are applied during one control period.

This article is organized as follows. Section II presents the model of the PMSM and two-level voltage source inverter. In Section III, the proposed FCS-MFPCC-I based on the ultralocal model and the improved FCS-MFPCC-II with two voltage vectors are presented. The simulation and experimental results are listed to verify the proposed FCS-MFPCC strategy in Section IV. Finally, a conclusion of this study is given in Section V.

II. Model of PMSM System

In this study, a surface PMSM that dq-axis inductance is equal is studied. The model in the rotating reference (dq) frame can be written as

$$\begin{cases} \frac{di_d}{dt} = \frac{1}{L_s}u_d - \frac{R_s}{L_s}i_d + \omega_r i_q \\ \frac{di_q}{dt} = \frac{1}{L_s}u_q - \frac{R_s}{L_s}i_q - \frac{1}{L_s}\left(L_s\omega_r i_d + \omega_r\psi_f\right) \end{cases} \tag{1}$$

where u_d and i_d are the d-axis stator voltage and current, respectively; u_q and i_q are the q-axis stator voltage and current, respectively; L_s is the stator inductance; R_s is the stator resistance; ω_r is the electrical rotor speed; and ψ_f is the flux linkage of the permanent magnet.

The PMSM is driven by a two-level three-phase voltage source inverter that has eight switching states. Therefore, the voltage can be calculated based on the different switching states as

$$U_s = 2U_{\rm dc}\left(S_A + S_B e^{j\frac{2\pi}{3}} + S_c e^{j\frac{4\pi}{3}}\right)/3 \tag{2}$$

where $U_{\rm dc}$ is the dc-link voltage; S_A, S_B, S_C are the switching states of the inverter.

According to (2), u_a, u_b, and u_c that are the a-phase, b-phase, and c-phase voltages can be derived with the eight different switching states, respectively, as shown in Fig. 1. Therefore, the voltages consist of the six active voltages (u_1–u_6) and two zero voltages (u_0, u_7).

III. Proposed FCS-MFPCC Algorithm

In the conventional FCS-MBPCC, the future current prediction is associated with the resistance, inductance, and flux linkage. The influence of the parameters is analyzed in [21]. The results indicated that parameters mismatch would increase

the current tracking errors and torque ripples. Therefore, to guarantee the robustness of the current-loop controller, a new method that can estimate and predict the current without using the motor parameters is proposed in this study.

A. Current Variations Estimation

In the proposed FCS-MFPCC, the future current prediction is based on the current variations that are deduced by the ultralocal model. The first-order ultralocal model of a single-input single-output system from [34] can be expressed as

$$\frac{dY(t)}{dt} = F(t) + \alpha U(t) \tag{3}$$

where $U(t)$ and $Y(t)$ are the system input and output variables, respectively; α is a scaling factor, and $F(t)$ represents the known and unknown parts of the system that contains the various terms.

Compared (3) with (1), the model of PMSM based on the ultralocal model can be rewritten as

$$\begin{cases} \frac{di_d}{dt} = F_d + \alpha u_d \\ \frac{di_q}{dt} = F_q + \alpha u_q \end{cases} \tag{4}$$

where $\alpha = \frac{1}{L_s}$, $F_q = -\frac{R_s}{L_s} i_q - \frac{1}{L_s}(L_s \omega_r i_d + \omega_r \varphi_f)$, $F_d = -\frac{R_s}{L_s} i_d + \omega_r i_q$.

In order to eliminate the influence of the parameters mismatch, F_d and F_q are assumed to be unknown. Based on (4), a sliding mode observer (SMO) that takes the unknown interference and parameters variation into account is designed to estimate the values F_d and F_q without using parameters. The details of the SMO are introduced in the Appendix.

Based on the first-order Euler and the discrete-time ultralocal model (4), the current variations $\Delta \boldsymbol{i_s}(k)|_j$ that are corresponding to the eight voltage vectors of the inverter can be derived as

$$\Delta \boldsymbol{i_s}(k)|_j = T_s \left[\boldsymbol{F_s}(k) + \alpha \boldsymbol{u_j}(k) \right], \quad j = 0, \ldots, 7 \tag{5}$$

where $\Delta \boldsymbol{i_s}(k) = \boldsymbol{i_s}(k+1) - \boldsymbol{i_s}(k)$ is the current variations during the (k)th control period; $\boldsymbol{i_s}(k+1)$ and $\boldsymbol{i_s}(k)$ are the currents at the $(k+1)$th and (k)th sampling period, respectively; $\boldsymbol{u_j}$ is the eight voltage vectors of the inverter, as shown in Fig. 1.

The current variations updating mechanism of the conventional FCS-MFPCC [29] and the proposed FCS-MFPCC is illustrated in Fig. 2. In the conventional FCS-MFPCC, only one current variation corresponding to the applied voltage vector can be updated at one control period while the others will not be updated. If a voltage is not selected over a period of time, its corresponding current variation cannot be updated in time, which may not be accurate for the future current prediction. Therefore, the delay and distortion of the current variations updating will affect the current tracking performance. Compared with the work in [30], the previous current variations are not involved in the LUT updating for the proposed FCS-MFPCC. Besides, a threshold needs to be set to avoid the several succeeding similar voltage vectors in [30], which may select the nonoptimal voltage vector if the two succeeding voltage vectors are similar. On the contrary, in the proposed FCS-MFPCC, based on (5) and the eight voltage vectors of the inverter, the current variations can be predicted and updated at every control period without using the previous values, as shown in Fig. 2(b).Therefore, the drawback of delay and distortion will be avoided, and the future current prediction will become more accurate.

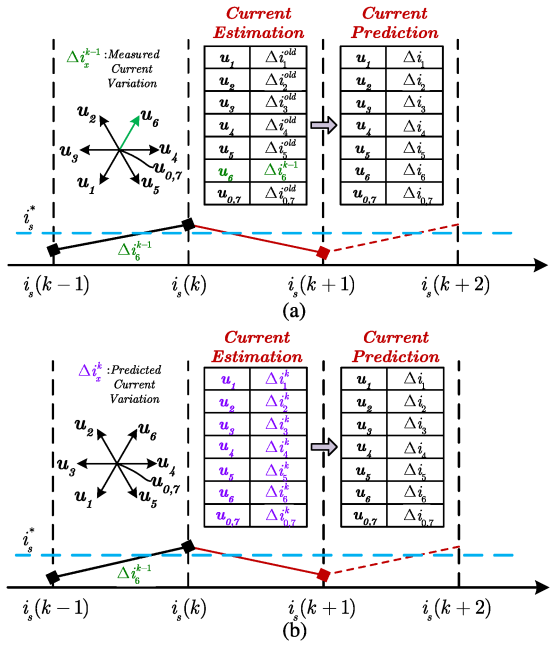

Fig. 2. Current variations updating mechanism of (a) the conventional FCS-MFPCC [29] and (b) the proposed FCS-MFPCC.

B. Future Current Prediction

Based on the principle of the FCS-MFPCC, the future currents $\boldsymbol{i_s}(k+1)$ and $\boldsymbol{i_s}(k+2)$ can be predicted as

$$\begin{cases} \boldsymbol{i_s}(k+1) = \boldsymbol{i_s}(k) + \Delta \boldsymbol{i_s}(k)|_{\boldsymbol{u}(k)} \\ \boldsymbol{i_s}(k+2) = \boldsymbol{i_s}(k+1) + \Delta \boldsymbol{i_s}(k+1)|_{\boldsymbol{u_j}(k+1)} \end{cases} \tag{6}$$

where $\boldsymbol{i_s}(k+2)$ is the predicted current at the $(k+2)$th sampling period; $\Delta \boldsymbol{i_s}(k)|_{\boldsymbol{u}(k)}$ is the estimated current variation at the (k)th sampling period that is corresponding to the voltage vector $\boldsymbol{u}(k)$; $\Delta \boldsymbol{i_s}(k+1)|_{\boldsymbol{u_j}(k+1)}$ is the predicted current variation at the $(k+1)$th sampling period by the eight voltage vectors. As we can see, the future current prediction is associated with the current variations. Inaccurate current variations will lead to more significant current ripples and even worsen the controller performance. Therefore, to accomplish the high accuracy of current tracking, accurate current variations must be guaranteed.

With (5) and (6), the future current at the $(k+1)$th sampling period can be estimated as

$$\begin{cases} i_d(k+1) = i_d(k) + T_s \left[\hat{F}_d(k) + \alpha u_d(k) \right] \\ i_q(k+1) = i_q(k) + T_s \left[\hat{F}_q(k) + \alpha u_q(k) \right] \end{cases} \tag{7}$$

where $\hat{F}_d(k)$ and $\hat{F}_q(k)$ are the observed values at the (k)th sampling period, respectively; $u_d(k)$ and $u_q(k)$ are the input voltages during the (k)th control period, respectively.

However, in the real digital implementation, the optimal voltage vector selected in the (k)th sampling period is not applied directly until the $(k+1)$th sampling period due to the one-step

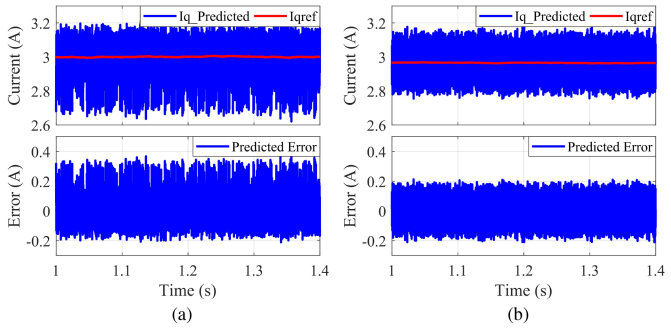

Fig. 3. Simulation results of the q-axis current prediction and predicted error. (a) Without compensation. (b) With two-step compensation.

delay of hardware. As a result, the selected voltage vector at the (k)th sampling period may not be the optimal voltage and even worsen the current tracking performance, as shown in Fig. 3. Therefore, it is important to compensate for the system delay with a two-step method [35]. According to the current and voltage at the $(k+1)$th, the future currents at the $(k+2)$th sampling period can be predicted as

$$\begin{cases} i_d\,(k+2)\,|_j = i_d\,(k+1) \\ \quad +T_s\left(\hat{F}_d\,(k+1) + \alpha u_d\,(k+1)|_j\right) \\ i_q\,(k+2)\,|_j = i_q\,(k+1) \\ \quad +T_s\left(\hat{F}_q\,(k+1) + \alpha u_q\,(k+1)|_j\right) \end{cases} \tag{8}$$

where $j = 0, \ldots, 6$; $u_d(k+1)|_j$ and $u_q(k+1)|_j$ are the projection of the seven voltage vectors in the dq-axis, respectively. In this study, only seven voltage vectors are selected to predict the future current. The reason for applying seven voltage vectors is that u_0 and u_7 have the same influence to the current when they are applied to the inverter. Therefore, in order to reduce the switching frequency, only the voltage u_0 is selected instead of u_7.

From (8), $\boldsymbol{i_s}(k+2)|_j$ can be calculated by seven different voltage vectors. Because the sampling period T_s is short enough, $\hat{F}_d$ and $\hat{F}_q$ at the $(k+1)$th sampling period are assumed equal to the value at the (k)th sampling period. Different from the conventional FCS-MBPCC, the future current prediction at the $(k+2)$th sampling period is only associated with the voltages, observer values, currents data and scaling factor without using the motor parameters. Therefore, the influence of the parameters mismatch can be reduced. Finally, based on the future currents, the optimal voltage vector u_{opt} can be selected by minimizing the cost function

$$Cf_j = \left[i_d^{\text{ref}} - i_d\,(k+2)|_j\right]^2 + \left[i_q^{\text{ref}} - i_q\,(k+2)|_j\right]^2 \tag{9}$$

where i_d^{ref} is the d-axis reference current that is set to 0; i_q^{ref} is the q-axis reference current that is deduced from the speed-loop controller. The structure diagram of the proposed FCS-MFPCC is shown in Fig. 4.

C. Two-Voltage-Vector Optimal Duration

In order to reduce the current ripples caused by applying a single voltage to the inverter during one control period, an optimal duty cycle modulation strategy of two vectors is studied in the proposed FCS-MFPCC strategy. Different from the conventional FCS-MFPCC, the two voltage vectors that are consisted of u_{opt} and u_0 are applied by the inverter to improve the steady-state performance. In this strategy, u_{opt} is the optimal voltage vector selected by the cost function and u_0 is the zero-voltage vector. However, in order to synthesize the optimal vector, the optimal duration plays a crucial role in decreasing the current tracking error. Based on the principle of the voltage vector synthesis and the optimal duration, the optimal voltage vector can be synthesized as

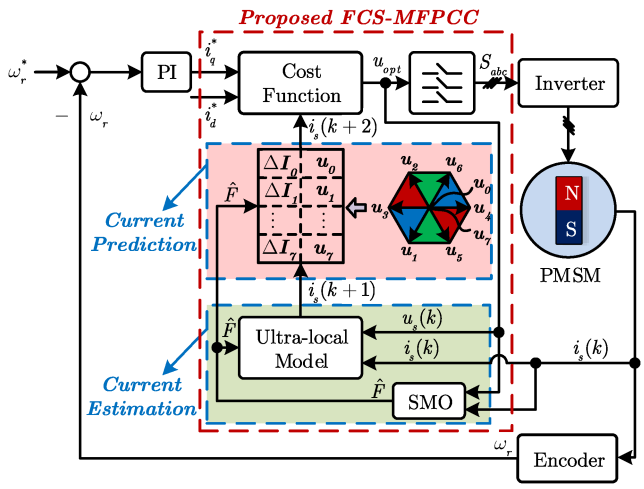

Fig. 4. Structure diagram of the proposed FCS-MFPCC.

$$\boldsymbol{u_s^{\text{opt}}} = \boldsymbol{u_{\text{opt}}} \odot \frac{t_{\text{opt}}}{T_s} + \boldsymbol{u_0} \odot \frac{(T_s - t_{\text{opt}})}{T_s} \tag{10}$$

where $\boldsymbol{u_s^{\text{opt}}}$ is the synthesized optimal voltage vector; t_{opt} is the optimal duration of the selected optimal voltage vector $\boldsymbol{u_{\text{opt}}}$; $\odot$ is the operator of Hadamard product.

In (10), the voltage vector $\boldsymbol{u_s^{\text{opt}}}$ is applied to improve the current tracking performance at the next control period. However, only eight voltage vectors of the inverter are known in the FCS-MFPCC strategy. Therefore, by replacing $\boldsymbol{i_s}(k+2)$ with $\boldsymbol{i_s^{\text{ref}}}$ in (4), the reference voltage vector $\boldsymbol{u_s^{\text{ref}}}$ can be derived with the discrete-time ultralocal model as

$$\boldsymbol{u_s^{\text{ref}}} = \frac{1}{\alpha}\left[\frac{\boldsymbol{i_s^{\text{ref}}} - \boldsymbol{i_s}\,(k+1)}{T_s} - \hat{\boldsymbol{F}}_{\boldsymbol{s}}\,(k+1)\right]. \tag{11}$$

In order to derive the optimal duration, another cost function is designed to minimize the error between the reference voltage vector $\boldsymbol{u_s^{\text{ref}}}$ and the synthesized optimal voltage vector $\boldsymbol{u_s^{\text{opt}}}$. The cost function J that considers t_{opt} as the independent variable can be designed as

$$J = \left|\boldsymbol{u_s^{\text{opt}}} - \boldsymbol{u_s^{\text{ref}}}\right|^2. \tag{12}$$

By solving the function $\partial J/\partial t_{\text{opt}} = 0$, the optimal duration of the selected optimal voltage vector can be calculated as

$$t_{\text{opt}} = \frac{\left(\boldsymbol{u_s^{\text{ref}}} - \boldsymbol{u_0}\right) \odot \left(\boldsymbol{u_{\text{opt}}} - \boldsymbol{u_0}\right)}{\left|\boldsymbol{u_{\text{opt}}} - \boldsymbol{u_0}\right|^2} \odot T_s. \tag{13}$$

However, if the adjacent voltage vector has a slight difference from each other, the optimal duration $t_{\rm opt}$ may exceed the current sampling period T_s, which will affect the future current compensation and even worsen the current tracking performance. Therefore, the limitation of the optimal duration $t_{\rm opt}$ is necessary to be set to guarantee the future current prediction. If $t_{\rm opt}$ exceeds the upper limit, T_s will be selected as the optimal duration. Similarly, if $t_{\rm opt}$ is below the lower limit, the 0 will be chosen as the optimal duration

$$t_{\rm opt} = \begin{cases} 0, & t_{\rm opt} < 0 \\ t_{\rm opt}, & 0 \le t_{\rm opt} \le T_s \\ T_s, & t_{\rm opt} > T_s. \end{cases} \tag{14}$$

Finally, with the optimal duration $t_{\rm opt}$ and the selected optimal voltage vector $u_{\rm opt}$, the reference voltage vector can be synthesized and applied at the next control period to improve the current tracking performance. Nevertheless, because of the optimal duration, the current variation corresponding to the applied voltage vector is not accurate for the future current estimation at the $(k+1)$th sampling period. Therefore, it is essential to compensate for the current variation during the (k)th control period to improve the accuracy of the future current prediction at the $(k+1)$th sampling period.

D. Current Correction at the (k+1)th Sampling Period

From (11), it is evident that the precision of the optimal duration is affected by the current value at the $(k+1)$th sampling period. Without using the zero-voltage vector, the conventional FCS-MFPCC estimates the current by using the voltage $u_d(k)$ and $u_q(k)$ that are imposed during the whole control period. However, because of the optimal duration, the selected voltage vector may not last for the whole control period. Therefore, the currents at the $(k+1)$th sampling period need to be corrected to decrease the current tracking error.

Based on (6), the current $\boldsymbol{i_s}(k+1)$ can be estimated with the current variation that is corresponding to the applied voltage $\boldsymbol{u_s}(k)$ during the (k)th control period. With the discrete-time ultralocal model, the current slope of the i_d and i_q at the (k)th sampling period can be rewritten as

$$\boldsymbol{m}_{\rm s\_opt}(k) = \left.\frac{d\boldsymbol{i_s}}{dt}\right|_{\boldsymbol{u_s(k)}} = \hat{\boldsymbol{F}}_{\boldsymbol{s}}(k) + \alpha \boldsymbol{u_s}(k) \tag{15}$$

where $\boldsymbol{m}_{\rm s\_opt}(k)$ is the dq-axis current slope that is corresponding to the voltage vector $\boldsymbol{u_s(k)}$ during the (k)th control period. Similarly, $\boldsymbol{m}_{\boldsymbol{s\_0}}(k)$ can be resolved with the voltage vectors $\boldsymbol{u_0}(k)$.

Finally, based on the optimal duration (13) and the current slope (15), the current variations during the (k)th control period can be calculated as

$$\Delta \boldsymbol{i_s}(k) = \boldsymbol{m}_{\rm s\_opt}(k) \odot t_{\rm opt}(k) + \boldsymbol{m}_{\boldsymbol{s\_0}}(k) \odot [T_s - t_{\rm opt}(k)] \tag{16}$$

where $t_{\rm opt}(k)$ is the optimal duration during the (k)th control period. Substituting (16) into (6), the current $\boldsymbol{i_s}(k+1)$ can be compensated with the corrected current variations.

The first step in the proposed FCS-MFPCC strategy is selecting the optimal voltage vector based on the cost function.

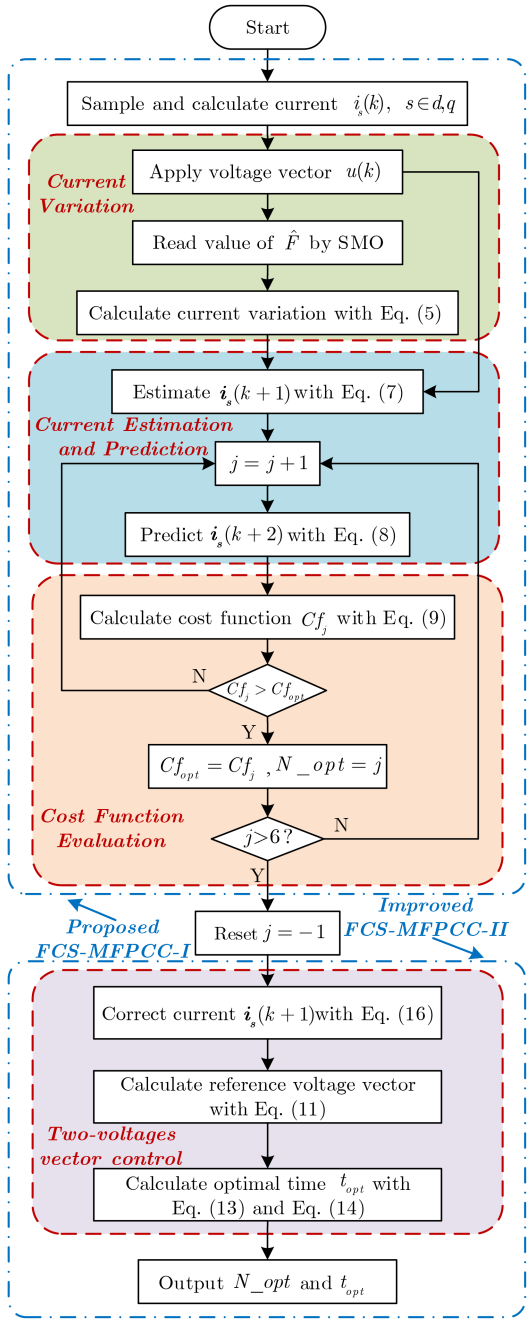

Fig. 5. Flowchart of the proposed FCS-MFPCC-I and the improved FCS-MFPCC-II.

Second, the optimal duration corresponding to the selected voltage vector is determined by (13). Finally, with the help of the optimal duration and the zero-voltage vector, the optimal voltage vector can be synthesized to reduce the current ripples. The flow chart of the proposed FCS-MFPCC that includes FCS-MFPCC-I and the improved FCS-MFPCC-II is shown in Fig. 5.

IV. Simulation and Experimental Results

To verify the effectiveness of the proposed FCS-MFPCC algorithm, simulations and experiments are carried out. The PMSM parameters are listed in Table I. The proposed FCS-MFPCC is

TABLE I
PARAMETERS OF PMSM

Symbol	Quantity	Value
p	Number of pole pairs	3
R_s	Stator resistance	0.675Ω
L_s	d-q axis inductance	0.0065 H
ψ_f	Permanent magnet flux	0.29 Wb
$U_{\rm dc}$	DC-bus voltage	100 V
P_N	Rate power	5.5 kW
I_N	Rate current	5 A

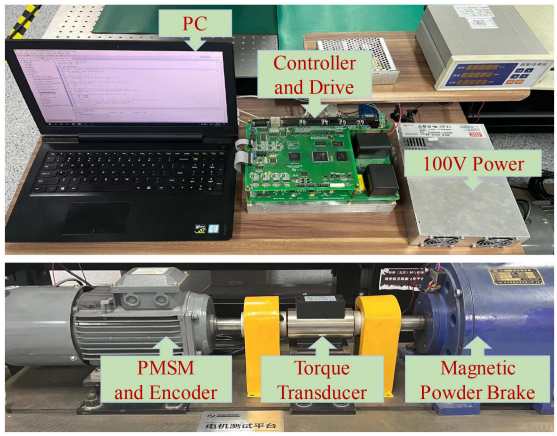

Fig. 6. PMSM experimental platform.

implemented on the platform that combines a TMS320F28335 DSP with a field programmable array (FPGA). The experimental platform is shown in Fig. 6. The FPGA is used to read encoder, converse A/D, and transmit data. The DSP is the core of the platform that is used to process the data from FPGA. The current sampling period in the simulation and DSP platform is 100μs. Apart from the proposed FCS-MFPCC with SMO (FCS-MFPCC-I) and the improved MFPCC with two voltage vectors (MFPCC-II), the conventional FCS-MBPCC (FCS-MBPCC) and FCS-MFPCC proposed in [29] (FCS-MFPCC-LUT) are introduced to verify the performance of the proposed FCS-MFPCC algorithm.

A. Simulation Results

Fig. 7 presents the stator current variations of the proposed FCS-MFPCC-I and FCS-MFPCC-LUT with different voltage vectors under 100-r/min speed and 2-N·m load. The current variations ΔI_d and ΔI_q correspond to the eight voltage vectors of the inverter. From Fig. 7(a), the delay and distortion of the current variations caused by imposing a nonoptimal voltage vector on the inverter affect the accuracy of the current prediction. In order to guarantee the accuracy of the current variations, if a voltage is not selected in more than 50 control periods, it will be selected at the next control period whether it is the optimal vector or not. Therefore, the error of the current prediction will be larger when the nonoptimal voltage vector is imposed. On the contrary, based on the ultralocal model, the current variations

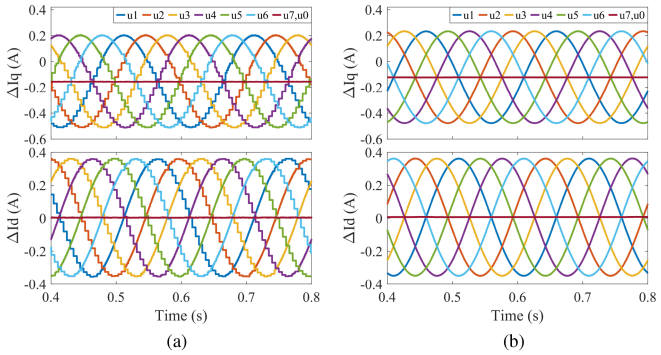

Fig. 7. Simulation results of the dq-axis current variations under different voltage vectors. (a) FCS-MFPCC-LUT. (b) Proposed FCS-MFPCC-I.

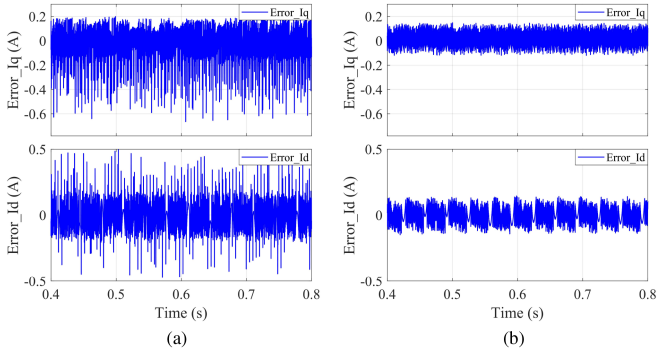

Fig. 8. Simulation results of the dq-axis current prediction error. (a) FCS-MFPCC-LUT. (b) Proposed FCS-MFPCC-I.

TABLE II
STEADY-STATE PERFORMANCE OF ACCURATE PARAMETERS

Method	$E_{\rm max}$ (A)	$E_{\rm std}$ (A)	THD
FCS-MBPCC	0.1969	0.0523	6.63%
FCS-MFPCC-LUT	0.7390	0.1393	13.57%
Proposed FCS-MFPCC-I	0.2007	0.0518	6.72%

can be calculated correctly at every control period without using the previous voltages. Therefore, the delay and distortion of the current variations can be eliminated, as shown in Fig. 7(b). As a consequence, compared with the FCS-MFPCC-LUT, the stator current prediction of the proposed FCS-MFPCC will be more accurate and the current error will be smaller than the FCS-MFPCC-LUT, as shown in Fig. 8.

The simulation results of the q-axis current (I_q) and three-phase current (I_{abc}) with the accurate parameters under 100 r/min and 2 N·m load are shown in Fig. 9, respectively. From Fig. 9(a) and (c), the q-axis current tracking performance of the proposed FCS-MFPCC-I has a small difference compared with the conventional FCS-MBPCC. However, because of the nonoptimal voltage vector, the current ripples of the FCS-MFPCC-LUT are more significant than the proposed FCS-MFPCC-I and the conventional FCS-MBPCC. Besides, in order to view the comparison intuitively, the quantitative values are summarized in Table II, which includes the max current error

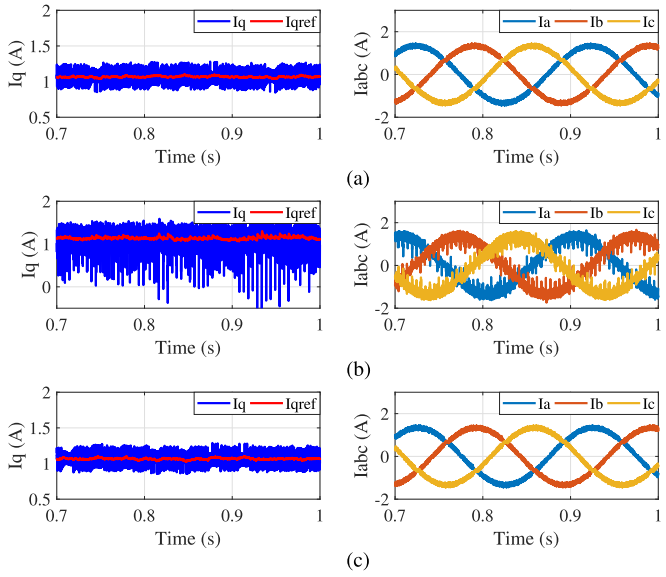

Fig. 9. Simulations results of the q-axis current and three-phase current steady-state performance with accurate parameters under $100\,\mathrm{r/min}$ with 2-$\mathrm{N{\cdot}m}$ load. (a) FCS-MBPCC. (b) FCS-MFPCC-LUT. (c) Proposed FCS-MFPCC-I.

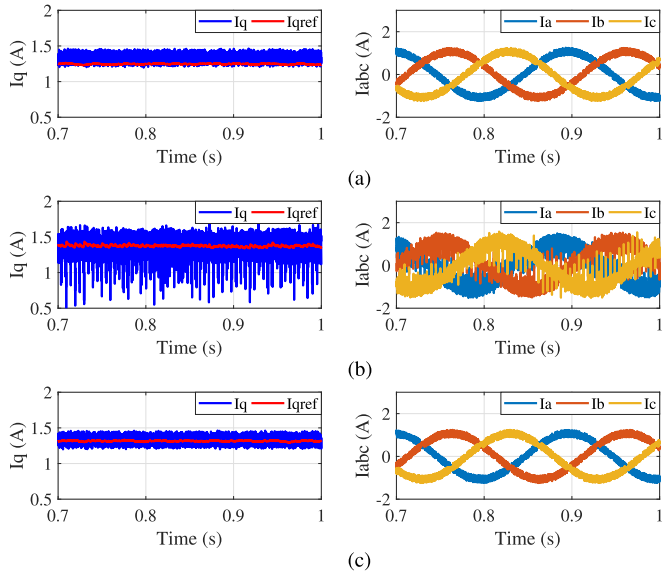

Fig. 10. Simulations results of the q-axis current and three-phase current steady-state performance with $50\%R_s$, 80%flux, and $150\%L_s$ under $100\,\mathrm{r/min}$ with 2-$\mathrm{N{\cdot}m}$ load. (a) FCS-MBPCC. (b) FCS-MFPCC-LUT. (c) Proposed FCS-MFPCC-I.

TABLE III
STEADY-STATE PERFORMANCE OF 50% R_s, 80% flux, AND 150% L_s

Method	$E_{\max}$ (A)	E_{std} (A)	THD
FCS-MBPCC	0.2148	0.0591	12.64%
FCS-MFPCC-LUT	0.9672	0.1123	18.14%
Proposed FCS-MFPCC-I	0.1439	0.0346	12.22%

($E_{\max}$), the standard deviation values of the error (E_{std}) (18), and the total harmonic distortions (THD) of the phase current. It is obvious that because the update frequency is increased, the THD of the proposed FCS-MFPCC-I is lower than the FCS-MFPCC-LUT

$$E_{\mathrm{mean}} = \frac{1}{n}\sum_{i=1}^{n} e(i) \tag{17}$$

$$E_{\mathrm{std}} = \sqrt{\frac{1}{n}\sum\nolimits_{i=1}^{n}\left[e(i) - E_{\mathrm{mean}}\right]^2} \tag{18}$$

where $e(i)$ is the q-axis current tracking error.

In order to verify the robustness of the proposed FCS-MFPCC, Fig. 10 shows the simulation results with the $50\%R_s$, $150\%L_s$, and 80%flux. In Fig. 10(a), it is obvious that the q-axis current of the FCS-MBPCC deviates from the reference current. The reason for this is that the future current prediction is dependent on the PMSM model, which will lead to an incorrect value when the parameters mismatch. On the contrary, different from the conventional FCS-MBPCC, based on the ultralocal model, the future current prediction of the proposed FCS-MFPCC-I is independent of the motor parameters. Therefore, compared with the conventional FCS-MBPCC, the proposed FCS-MFPCC-I has better current tracking performance and lower THD of the phase current, as shown in Fig. 10(c) and Table III.

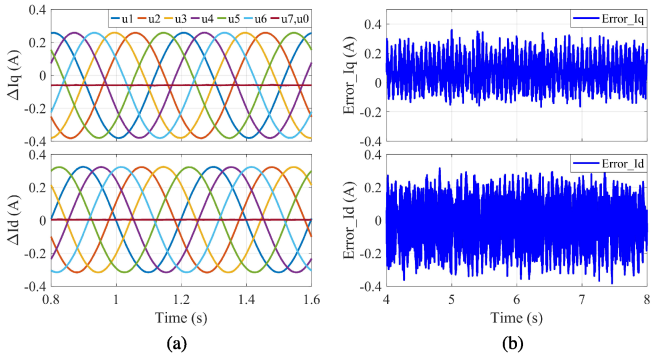

Fig. 11. Experimental results of (a) current variations and (b) prediction error in dq-axis of the proposed FCS-MFPCC-I under different voltage vectors.

From the simulation results, the performance of the proposed FCS-MFPCC-I is verified preliminary by comparing with the other strategies under different working conditions. Without using the parameters, the robustness of the proposed FCS-MFPCC-I is improved when the parameters mismatch.

B. Experimental Results

In order to analyze the results of the proposed FCS-MFPCC-I and the improved FCS-MFPCC-II strategies, the current information is measured by sensors and stored in PC from the serial communication.

1) Current Variations and Predicted Error: Fig. 11 shows the experimental results of the dq-axis current variations (a) and predicted error (b) for the proposed FCS-MFPCC-I under different voltage vectors. As shown in Fig. 11(a), Similar to the simulation results, the delay and distortion that exist in the dq-axis current variations updating are solved by updating the current variations at every control period. Therefore, the

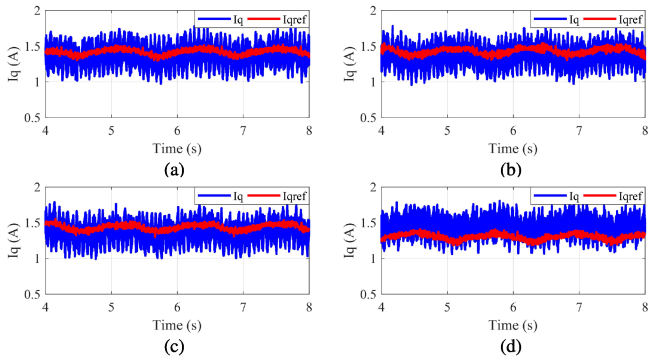

Fig. 12. Experimental results of steady-state performance of q-axis current for conventional MBPCC with parameters variation under $100\,\mathrm{r/min}$ with 2-$\mathrm{N{\cdot}m}$ load. (a) MBPCC with $50\%R_s$. (b) MBPCC with 80%flux. (c) MBPCC with $150\%L_s$. (d) MBPCC with $50\%R_s$, 80%flux, and $150\%L_s$.

accuracy of the future current prediction can be guaranteed to decrease the predicted error, as shown in Fig. 11(b).

2) Robustness of the Conventional FCS-MBPCC: In order to verify the performance of the conventional FCS-MBPCC influenced by the parameters mismatch, the experimental results with the parameters variation are shown in Fig. 12. As can be seen, it is obvious that the q-axis current (I_q) deviates from the reference value when the parameters vary from the nominal value, as shown in Fig. 12(a)–(d). With the parameters mismatch, the current tracking performance is affected. Similar to the results studied in [21], compared with the resistance and flux, the inductance mismatch has a more severe influence on the current prediction. Nevertheless, because the torque is proportional to the q-axis current, the torque ripples can be more significant with the q-axis current deviation. Therefore, to guarantee the stability of the output torque, it is necessary to improve the robustness of the conventional FCS-MBPCC.

3) Dynamic Performance of the Designed SMO: As can be seen from (4), the parameters F_d and F_q are associated with the electrical rotor speed and the q-axis current. Therefore, in order to verify the dynamic performance of the designed SMO, the experiments are carried out under the speed step from $50\,\mathrm{r/min}$ to $100\,\mathrm{r/min}$ at $5\,\mathrm{s}$ and load step from $0\,\mathrm{N{\cdot}m}$ to $2\,\mathrm{N{\cdot}m}$ at $5\,\mathrm{s}$, respectively. As can be seen from Fig. 13(a), when the speed step is at $5\,\mathrm{s}$, the designed SMO can respond to the speed step fast. The settling time of the designed SMO for F_d and F_q is $778\,\mathrm{ms}$ and $772\,\mathrm{ms}$, respectively, which is almost the same as the speed settling time. Similarly, when the load step is at $5\,\mathrm{s}$, the designed SMO for F_d and F_q can also fast respond to the q-axis current step, which is $840\,\mathrm{ms}$ and $845\,\mathrm{ms}$, respectively, as shown in Fig. 13(b). Therefore, the parameters F_d and F_q can be effectively observed based on the designed SMO.

4) Steady-State Performance of the Proposed FCS-MFPCC Strategy: In order to further verify the steady-state performance of the proposed FCS-MFPCC-I and the improved FCS-MFPCC-II, a comparative experiment with the conventional FCS-MBPCC under $100L_s$ and $150L_s$ is carried out, and the results are shown in Figs. 14 and 15, respectively. From top to bottom, the experimental results include the q-axis current (I_q), there-phase current (I_{abc}) and the A-phase current fast Fourier

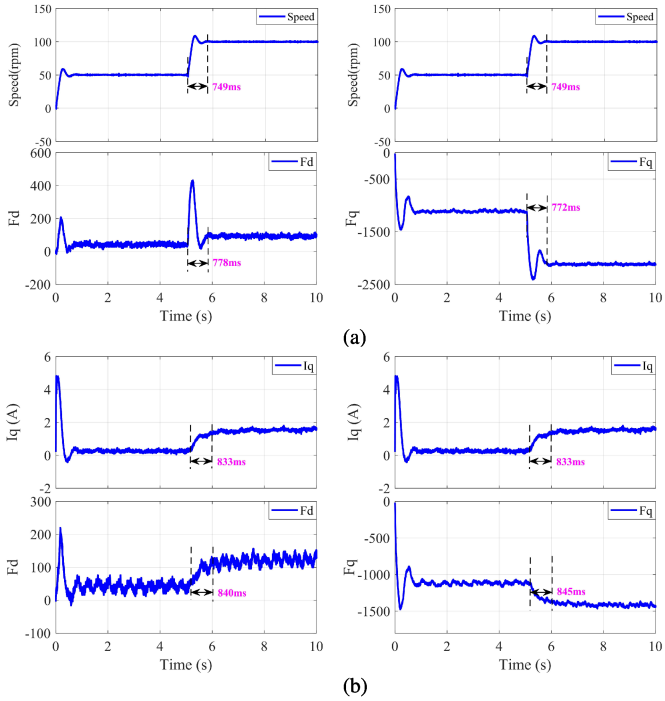

Fig. 13. Experimental results of the observed values F_d and F_q under different working conditions. (a) Speed step. (b) Load step.

transform analysis, respectively. Comparing Fig. 14(a) and (b) with Fig. 15(a) and (b), it is obvious that the steady-state current tracking performance of the conventional FCS-MBPCC will be deteriorated when the inductance mismatch. On the contrary, based on the discrete-time ultralocal model, the current variations can be updated without using the parameters. Therefore, when the parameters mismatch, the proposed FCS-MFPCC-I can still track the reference current effectively. However, because the scaling factor is changed to simulate the parameters mismatch, the designed SMO may slightly influence the future current prediction. Besides, when the inductance mismatch, the A-phase current THD of conventional FCS-MBPCC increases from 3.9684% to 7.1021%, whereas the A-phase current THD of the proposed FCS-MFPCC has slight differences, which increases from 4.1001% to 5.2574%.

However, the current ripples still can influence the controller performance if a voltage vector is applied during a whole control period. Therefore, in order to reduce the current ripples, the two-voltage-vector strategy is studied in this study. As can be seen from Fig. 14(c), by applying two voltage vectors during one control period, the current tracking performance of the improved FCS-MFPCC-II is better than the conventional FCS-MBPCC and the proposed FCS-MFPCC-I. Besides, benefiting from the synthesized optimal voltage vector, the THD of the improved FCS-MFPCC-II is decreased to 3.4519% compared with the proposed FCS-MFPCC-I and the conventional FCS-MBPCC. In the proposed FCS-MFPCC-II, the amplitude of the synthesized optimal voltage vector can be adjusted with the optimal duration by introducing a zero-voltage vector into the active voltage vector. Therefore, the future current can be predicted more accurately, which results

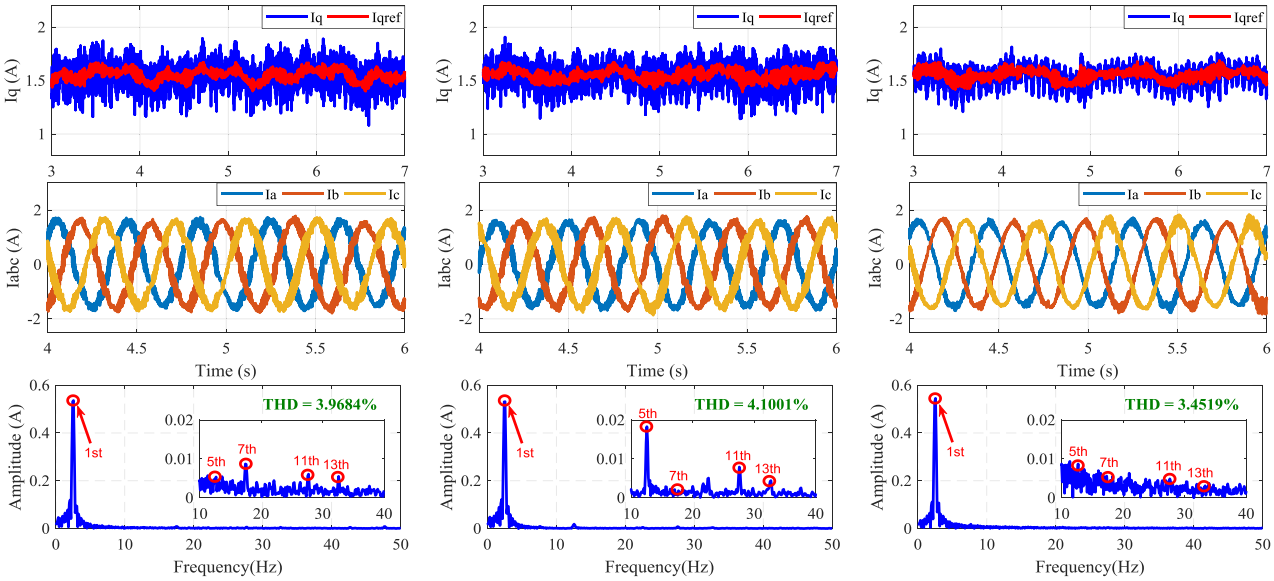

Fig. 14. Experimental results of the steady-state performance under $100\%L_s$ at $50\,\mathrm{r/min}$ and 2- $\mathrm{N{\cdot}m}$ condition. (a) Conventional FCS-MBPCC. (b) Proposed FCS-MFPCC-I. (c) Proposed FCS-MFPCC-II.

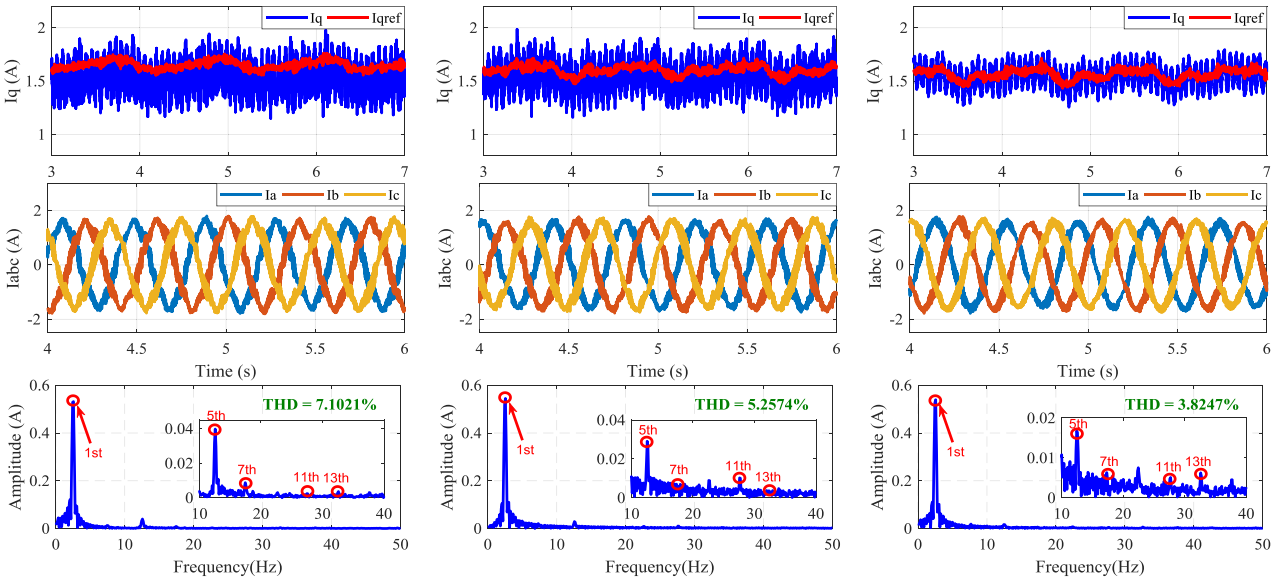

Fig. 15. Experimental results of the steady-state performance under $150\%L_s$ at $50\,\mathrm{r/min}$ and $2\,\mathrm{N{\cdot}m}$ condition. (a) Conventional FCS-MBPCC. (b) Proposed FCS-MFPCC-I. (c) Improved FCS-MFPCC-II.

in much less harmonic current and lowering the stator current THD.

5) Step Tracking Performance of the Proposed FCS-MFPCC Strategy: Based on the discrete-time ultralocal model, the current variations can be updated at every control period without using the motor parameters. However, as can be seen from (4), the scaling factor α is associated with the inductance parameter, which may affect the dynamic performance when tracking the step reference. Therefore, the experiments of the q-axis reference current step are carried out with the inductance mismatch to verify the dynamic performance of the proposed FCS-MFPCC-I and the improved FCS-MFPCC-II. The experimental results are shown in Figs. 16–18.

In the conventional FCS-MBPCC, the future current prediction is based on the motor model, which can directly change the parameters in the controller to simulate the parameters mismatch. On the contrary, in the proposed FCS-MFPCC strategy, the future current prediction is independent of the motor parameters, which cannot directly change the parameters in the controller. However, because the scaling factor α is associated with the inductance, the inductance mismatch can be simulated by varying the scaling factor in our study.

As shown in Figs. 16–18, the q-axis reference current step from $0\,\mathrm{A}$ to $1\,\mathrm{A}$ at $3\,\mathrm{s}$. When the actual parameter values are matched with the nominal values, the three strategies can

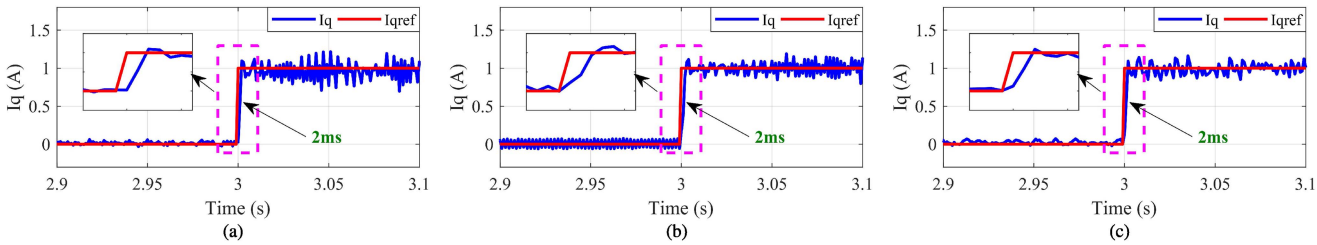

Fig. 16. Experimental results of the dynamic performance with the q-axis reference current step under $100\%L_s$ condition. (a) Conventional FCS-MBPCC. (b) Proposed FCS-MFPCC-I. (c) Proposed FCS-MFPCC-II.

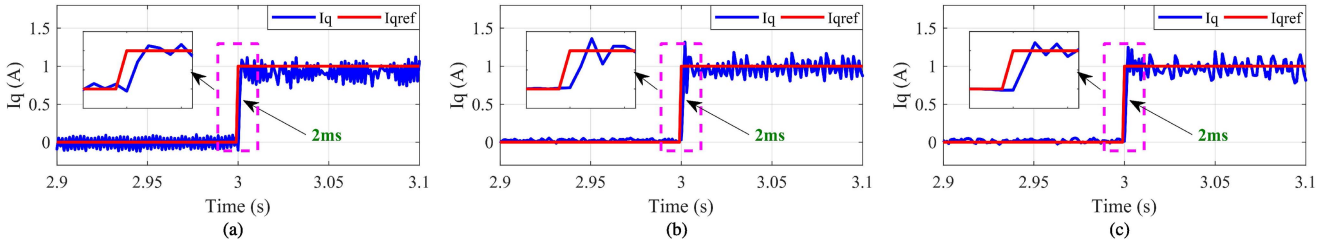

Fig. 17. Experimental results of the dynamic performance with the q-axis reference current step under $150\%L_s$ condition. (a) Conventional FCS-MBPCC. (b) Proposed FCS-MFPCC-I. (c) Proposed FCS-MFPCC-II.

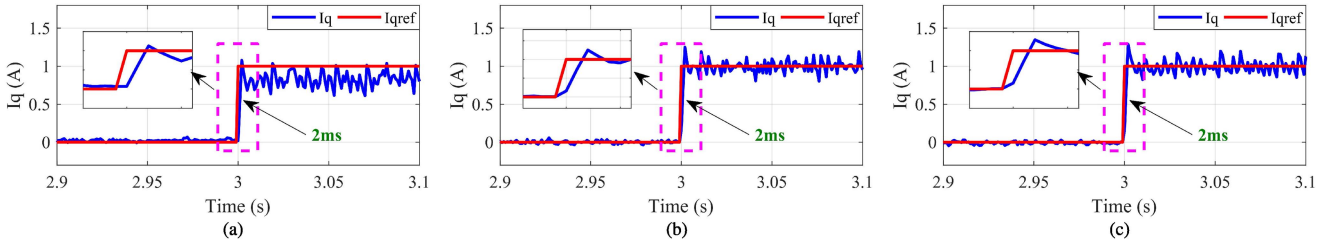

Fig. 18. Experimental results of the dynamic performance with the q-axis reference current step under $50\%L_s$ condition. (a) Conventional FCS-MBPCC. (b) Proposed FCS-MFPCC-I. (c) Proposed FCS-MFPCC-II.

effectively track the reference current, and the response time is similar to each other, which is $2\,\mathrm{ms}$. However, because of the inductance parameter mismatch, although the response time is not changed, the current tracking performance is decreased with the inaccurate future current prediction in the conventional FCS-MBPCC. Meanwhile, in the proposed FCS-MFPCC strategy, because the future currents prediction is independent of the motor parameters, the reference current still can be effectively tracked when the parameters mismatch. However, because the scaling factor α is associated with the inductance, the overshoot may occur with the reference current step. Therefore, the scaling factor α needs to be selected carefully to guarantee the dynamic performance of the proposed FCS-MFPCC strategy.

6) Dynamic Performance of the Proposed FCS-MFPCC Strategy: The transient behavior of the proposed FCS-MFPCC strategies is further tested under a speed step from $50\,\mathrm{r/min}$ to $100\,\mathrm{r/min}$ at $5\,\mathrm{s}$ and a load step from $0\,\mathrm{N{\cdot}m}$ to $2\,\mathrm{N{\cdot}m}$ at $10\,\mathrm{s}$. The experimental results of the proposed FCS-MFPCC strategies dynamic performance are shown in Fig. 19. From top to the bottom, the experimental results include the q-axis current response (I_q), a-phase current response (I_a), and the speed response ($Speed$), respectively. As can be seen from Fig. 19, whether the speed step or the load step, the proposed FCS-MFPCC-I and the improved FCS-MFPCC-II can respond to the step fast and track the reference current effectively, which has a similar performance to the conventional FCS-MBPCC. Besides, the proposed FCS-MFPCC strategies have excellent speed performance that can limit the speed tracking error within $\pm 2\mathrm{r/min}$.

7) Proposed FCS-MFPCC Strategy Performance Analysis: In order to evaluate the response time and current tracking performance, the integral of time and absolute error (ITAE) index, as shown in (19) [36], is studied to compare the performance of the conventional FCS-MBPCC and the proposed FCS-MFPCC

$$\mathrm{ITAE} = \int t\,|e(t)|\,dt \tag{19}$$

where $e(t)$ is the q-axis current tracking error.

Fig. 20 shows the experimental results of the q-axis current ITAE values within $2\,\mathrm{s}$ at $50\,\mathrm{r/min}$ under inductance mismatch

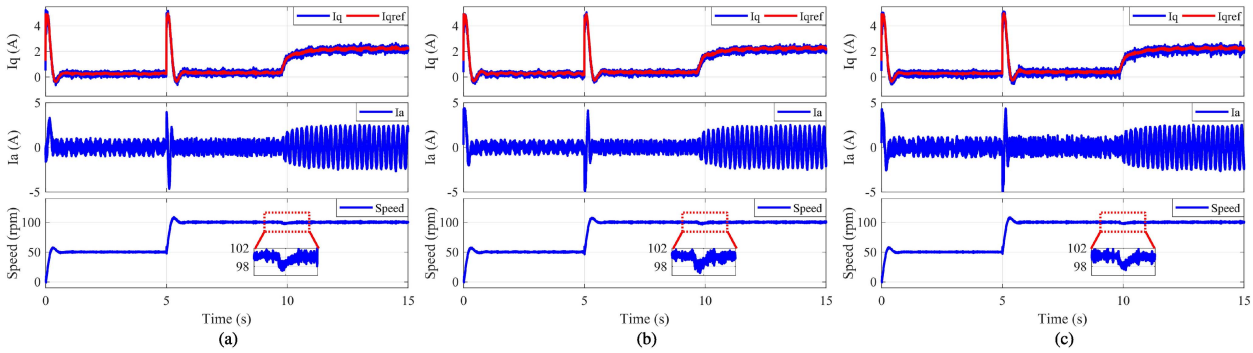

Fig. 19. Experimental results of the dynamic performance with the speed and load step. (a) Conventional FCS-MBPCC. (b) Proposed FCS-MFPCC-I. (c) Proposed FCS-MFPCC-II.

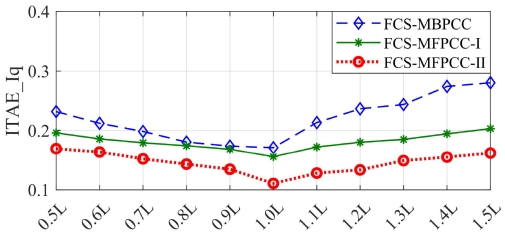

Fig. 20. Experimental results of q-axis current ITAE values under inductance mismatch.

TABLE IV
COMPUTATION BURDEN COMPARISON

Method	Average Computational Time	Clock Cycles
Conventional FCS-MBPCC	35.58μs	5337
Proposed FCS-MFPCC-I	31.19μs	4679
Improved FCS-MFPCC-II	32.09μs	4814

for the conventional FCS-MBPCC, the proposed FCS-MFPCC-I, and the improved FCS-MFPCC-II. The range of inductance mismatch is $\pm 50\%$. As can be seen from Fig. 20, it is obvious that the inductance mismatch severely affects the conventional FCS-MBPCC because its future current prediction is dependent on the motor model. On the contrary, in the proposed FCS-MFPCC strategies, the future current prediction is based on the ultralocal model without using the motor parameters. Meanwhile, by applying two voltage vectors to synthesize the optimal voltage vector, the current tracking error can be decreased in the improved FCS-MFPCC-II, which has a lower q-axis current ITAE value compared with the conventional FCS-MBPCC and the proposed FCS-MFPCC-I.

8) Computational Burden Comparison: In order to validate the performance of the proposed FCS-MFPCC for real-time implementation, the computational time is compared in Table IV. For the TMS320F28335(DSP), the main frequency is 150 MHz. Therefore, based on the clock cycles, the computational time can be calculated. In the conventional FCS-MBPCC, the current variations are deduced with the PMSM model, which can increase the computational burden. On the contrary, based on the ultralocal model, the computational efficiency is improved in the proposed FCS-MFPCC-I. The average computational time is decreased from 35.58 μs to 31.19 μs. Besides, although the two vectors are applied in the improved FCS-MFPCC-II, the computational time only increases by 1.1 μs. Therefore, the improved FCS-MFPCC-II can improve the current tracking performance without increasing the computational burden.

Therefore, based on the analysis in the time domain and frequency domain, it can be concluded that the improved MFPCC-II strategy that is independent of the parameters has better performance with the two voltage vectors and the compensation strategy.

V. CONCLUSION

In this article, a two-vector-based finite control set MFPCC strategy with an improved current variations updating mechanism is studied. The simulation and experimental results show that the proposed FCS-MFPCC-I and the conventional FCS-MBPCC have a similar current tracking performance when the motor parameters are accurate. However, when the parameters mismatch, the proposed FCS-MFPCC-I has better dynamic and steady-state current tracking performance than the conventional FCS-MBPCC. Besides, compared with the FCS-MFPCC-LUT, the drawback of delay and distortion in the current variations update can be avoided by updating the current variations at every control period. Furthermore, compared with the proposed FCS-MFPCC-I, the improved FCS-MFPCC-II has smaller ITAE values and lower current ripples because of the synthesized optimal voltage vector and the compensate strategy. Finally, the simulation and experimental results verified that the proposed FCS-MFPCC-I and the improved FCS-MFPCC-II have better parameter robustness and excellent dynamic and steady-state performance. In addition, the scaling factor α is worthy of further study to guarantee the accuracy of the future current prediction.

V. APPENDIX

In the proposed FCS-MFPCC, F_d and F_q affect the accuracy of the current prediction. Therefore, it is important to estimate

F_d and F_q. In this study, an SMO that has the advantage of easy implementation is designed to observe the value of F_d and F_q.

From (4), based on the PMSM model and ultralocal model, the SMO can be constructed as

$$\begin{cases} \dot{\hat{\boldsymbol{i}}}_{\boldsymbol{s}} = \hat{\boldsymbol{F}} + \alpha \boldsymbol{u}_{\boldsymbol{s}} + \boldsymbol{y} \\ \dot{\hat{\boldsymbol{F}}} = \xi \boldsymbol{y} \end{cases} \tag{A1}$$

where $\hat{\boldsymbol{i}}_{\boldsymbol{s}}$ and $\hat{\boldsymbol{F}}$ are the estimations of the stator current and F, respectively; ξ is the control law gain coefficient; $\boldsymbol{y}$ is the function that guarantees the current error between the real value and observed value converge to 0.

The sliding mode surface in the proposed SMO is as follows:

$$s = \boldsymbol{e_i} = \boldsymbol{i_s} - \hat{\boldsymbol{i}}_{\boldsymbol{s}} \tag{A2}$$

where e_i is the stator current error.

With the condition of (A3)

$$\boldsymbol{y} = -\beta \operatorname{sign}(\boldsymbol{e_i}) \tag{A3}$$

the derivation of the sliding mode surface s can be derived as

$$\dot{s} = \dot{\boldsymbol{i}}_{\boldsymbol{s}} - \dot{\hat{\boldsymbol{i}}}_{\boldsymbol{s}} = \boldsymbol{e_f} - \boldsymbol{y} = \boldsymbol{e_f} + \beta \operatorname{sign}(\boldsymbol{e_i}) \tag{A4}$$

where $\operatorname{sign}(\cdot)$ is the sign function and β is the scale factor.

In order to guarantee the condition of asymptotic stability, in this study, the values of β and ξ are set to 500 and 30, respectively.

REFERENCES

[1] J. Liu, H. Li, and Y. Deng, "Torque ripple minimization of PMSM based on robust ILC via adaptive sliding mode control," *IEEE Trans. Power Electron.*, vol. 33, no. 4, pp. 3655–3671, Apr. 2018.

[2] Y. Deng, J. Wang, H. Li, J. Liu, and D. Tian, "Adaptive sliding mode current control with sliding mode disturbance observer for PMSM drives," *ISA Trans.*, vol. 88, pp. 113–126, May 2019.

[3] M. Huang, Y. Deng, H. Li, and J. Wang, "Torque ripple suppression of PMSM using fractional-order vector resonant and robust internal model control," *IEEE Trans. Transp. Elect.*, vol. 7, no. 3, pp. 1437–1453, Sep. 2021.

[4] W. Xie et al., "Finite-control-Set model predictive torque control with a deadbeat solution for PMSM drives," *IEEE Trans. Ind. Electron.*, vol. 62, no. 9, pp. 5402–5410, Sep. 2015.

[5] Y. Wang et al., "Deadbeat model-predictive torque control with discrete space-vector modulation for PMSM drives," *IEEE Trans. Ind. Electron.*, vol. 64, no. 5, pp. 3537–3547, May 2017.

[6] T. Tarczewski and L. M. Grzesiak, "Constrained state feedback speed control of PMSM based on model predictive approach," *IEEE Trans. Ind. Electron.*, vol. 63, no. 6, pp. 3867–3875, Jun. 2016.

[7] M. Khalilzadeh, S. Vaez-Zadeh, J. Rodriguez, and R. Heydari, "Model-free predictive control of motor drives and power converters: A review," *IEEE Access*, vol. 9, pp. 105733–105747, 2021.

[8] M. Khalilzadeh, S. Vaez-Zadeh, and M. S. Eslahi, "Parameter-free predictive control of IPM motor drives with direct selection of optimum inverter voltage vectors," *IEEE J. Emerg. Sel. Topics Power Electron.*, vol. 9, no. 1, pp. 327–334, Feb. 2021.

[9] X. Yuan, Y. Zuo, Y. Fan, and C. H. T. Lee, "Model-free predictive current control of SPMSM drives using extended state observer," *IEEE Trans. Ind. Electron.*, vol. 68, no. 2, pp. 993–1003, Feb. 2021.

[10] P. G. Carlet, F. Tinazzi, S. Bolognani, and M. Zigliotto, "An effective model-free predictive current control for synchronous reluctance motor drives," *IEEE Trans. Ind. Appl.*, vol. 55, no. 4, pp. 3781–3790, Jul./Aug. 2019.

[11] P. Cortes, J. Rodriguez, C. Silva, and A. Flores, "Delay compensation in model predictive current control of a three-phase inverter," *IEEE Trans. Ind. Electron.*, vol. 59, no. 2, pp. 1323–1325, Feb. 2012.

[12] F. Morel, X. Lin-Shi, J.-M. Retif, B. Allard, and C. Buttay, "A comparative study of predictive current control schemes for a permanent-magnet synchronous machine drive," *IEEE Trans. Ind. Electron.*, vol. 56, no. 7, pp. 2715–2728, Jul. 2009.

[13] H. Miranda, P. Cortes, J. Yuz, and J. Rodriguez, "Predictive torque control of induction machines based on state-space models," *IEEE Trans. Ind. Electron.*, vol. 56, no. 6, pp. 1916–1924, Jun. 2009.

[14] J. Wang, F. Wang, Z. Zhang, S. Li, and J. Rodríguez, "Design and implementation of disturbance compensation-based enhanced robust finite control set predictive torque control for induction motor systems," *IEEE Trans. Ind. Informat.*, vol. 13, no. 5, pp. 2645–2656, Oct. 2017.

[15] M. Preindl and S. Bolognani, "Model predictive direct speed control with finite control set of PMSM drive systems," *IEEE Trans. Power Electron.*, vol. 28, no. 2, pp. 1007–1015, Feb. 2013.

[16] Y. Zhou, H. Li, H. Zhang, J. Mao, and J. Huang, "Model free deadbeat predictive speed control of surface-mounted permanent magnet synchronous motor drive system," *J. Elect. Eng. Technol.*, vol. 14, no. 1, pp. 265–274, Jan. 2019.

[17] J. Rodriguez et al., "Predictive current control of a voltage source inverter," *IEEE Trans. Ind. Electron.*, vol. 54, no. 1, pp. 495–503, Feb. 2007.

[18] B. Wang, X. Chen, Y. Yu, G. Wang, and D. Xu, "Robust predictive current control with online disturbance estimation for induction machine drives," *IEEE Trans. Power Electron.*, vol. 32, no. 6, pp. 4663–4674, Jun. 2017.

[19] Y. Yao, Y. Huang, F. Peng, J. Dong, and H. Zhang, "An improved deadbeat predictive current control with online parameter identification for surface-mounted PMSMs," *IEEE Trans. Ind. Electron.*, vol. 67, no. 12, pp. 10145–10155, Dec. 2020.

[20] M. Siami, D. A. Khaburi, and J. Rodríguez, "Torque ripple reduction of predictive torque control for PMSM drives with parameter mismatch," *IEEE Trans. Power Electron.*, vol. 32, no. 9, pp. 7160–7168, Sep. 2017.

[21] X. Zhang, L. Zhang, and Y. Zhang, "Model predictive current control for PMSM drives with parameter robustness improvement," *IEEE Trans. Power Electron.*, vol. 34, no. 2, pp. 1645–1657, Feb. 2019.

[22] X. Yuan, S. Zhang, and C. Zhang, "Improved model predictive current control for SPMSM drives with parameter mismatch," *IEEE Trans. Ind. Electron.*, vol. 67, no. 2, pp. 852–862, Feb. 2020.

[23] Y. Zhou, S. Zhang, C. Zhang, X. Li, X. Li, and X. Yuan, "Current prediction error based parameter identification method for SPMSM with deadbeat predictive current control," *IEEE Trans. Energy Convers.*, vol. 36, no. 3, pp. 1700–1710, Sep. 2021.

[24] X. Zhang, B. Hou, and Y. Mei, "Deadbeat predictive current control of permanent-magnet synchronous motors with stator current and disturbance observer," *IEEE Trans. Power Electron.*, vol. 32, no. 5, pp. 3818–3834, May 2017.

[25] D. Q. Dang, M. S. Rafaq, H. H. Choi, and J.-W. Jung, "Online parameter estimation technique for adaptive control applications of interior PM synchronous motor drives," *IEEE Trans. Ind. Electron.*, vol. 63, no. 3, pp. 1438–1449, Mar. 2016.

[26] N. Jabbour and C. Mademlis, "Online parameters estimation and autotuning of a discrete-time model predictive speed controller for induction motor drives," *IEEE Trans. Power Electron.*, vol. 34, no. 2, pp. 1548–1559, Feb. 2019.

[27] C. Xu, Z. Han, and S. Lu, "Deadbeat predictive current control for permanent magnet synchronous machines with closed-form error compensation," *IEEE Trans. Power Electron.*, vol. 35, no. 5, pp. 5018–5030, May 2020.

[28] C.-K. Lin, T.-H. Liu, J.-T. Yu, L.-C. Fu, and C.-F. Hsiao, "Model-free predictive current control for interior permanent-magnet synchronous motor drives based on current difference detection technique," *IEEE Trans. Ind. Electron.*, vol. 61, no. 2, pp. 667–681, Feb. 2014.

[29] C.-K. Lin, J.-T. Yu, Y.-S. Lai, and H.-C. Yu, "Improved model-free predictive current control for synchronous reluctance motor drives," *IEEE Trans. Ind. Electron.*, vol. 63, no. 6, pp. 3942–3953, Jun. 2016.

[30] C. Ma, H. Li, X. Yao, Z. Zhang, and F. De Belie, "An improved model-free predictive current control with advanced current gradient updating mechanism," *IEEE Trans. Ind. Electron.*, vol. 68, no. 12, pp. 11968–11979, Dec. 2021.

[31] F. Yu, C. Zhou, X. Liu, and C. Zhu, "Model-free predictive current control for three-level inverter-fed IPMSM with an improved current difference updating technique," *IEEE Trans. Energy Convers.*, vol. 36, no. 4, pp. 3334–3343, Dec. 2021.

[32] Y. Zhang, J. Jin, and L. Huang, "Model-free predictive current control of PMSM drives based on extended state observer using ultralocal model," *IEEE Trans. Ind. Electron.*, vol. 68, no. 2, pp. 993–1003, Feb. 2021.
[33] Y. Zhou, H. Li, and H. Zhang, "Model-free deadbeat predictive current control of a surface-mounted permanent magnet synchronous motor drive system," *J. Power Electron.*, vol. 18, no. 1, pp. 103–115, 2018.
[34] M. Fliess and C. Join, "Model-free control," *Int. J. Control*, vol. 86, pp. 2228–2252, May 2013.
[35] Y. Zuo, J. Mei, C. Jiang, and C. H. T. Lee, "Digital implementation of deadbeat-direct torque and flux control for permanent magnet synchronous machines in the M–T reference frame," *IEEE Trans. Power Electron.*, vol. 36, no. 4, pp. 4610–4621, Apr. 2021.
[36] A. Bartoszewicz and A. Nowacka-Leverton, "ITAE optimal sliding modes for third-order systems with input signal and state constraints," *IEEE Trans. Automat. Control*, vol. 55, no. 8, pp. 1928–1932, Aug. 2010.

Zheng Sun (Graduate Student Member, IEEE) was born in Henan, China, in 1998. He received the B.E. degree in mechanical design, manufacturing and automation from Sichuan University, Chengdu, China, in 2019. He is currently working toward the Ph.D. degree in mechatronic engineering with the University of Chinese Academy of Sciences, Beijing, China, and the Changchun Institute of Optics, Fine Mechanics and Physics, Chinese Academy of Sciences, Changchun, China.

His research interests include motor drives, model predictive control, sliding-mode control, and digital control implemented with DSP.

Yongting Deng (Senior Member, IEEE) was born in Shandong, China, in 1987. He received the B.E. degree in automation from the China University of Petroleum, Beijing, China, in 2010, and the M.S. degree in mechatronic engineering and Ph.D. degree in mechatronic engineering from the Changchun Institute of Optics, Fine Mechanics and Physics, Chinese Academy of Sciences, Changchun, China, in 2015.

He is currently an Associate Professor with the Changchun Institute of Optics, Fine Mechanics and Physics, Chinese Academy of Sciences. He has authored or coauthored more than 50 publications in the research interests that include controller design for ac motor drives and linear motor drives, intelligent control, and high-precision machine control techniques.

Jianli Wang (Member, IEEE) was born in Shandong, China, in 1971. He received the Ph.D. degree in mechatronic engineering from the Changchun Institute of Optics, Fine Mechanics and Physics, Chinese Academy of Sciences, Changchun, China, in 2002.

He is currently a Professor with the Changchun Institute of Optics, Fine Mechanics and Physics, Chinese Academy of Sciences. He has authored or coauthored more than 100 publications in his main areas of research, which are optical-electric telescope, high-resolution imaging, and high-precision machine control techniques.

Tian Yang (Graduate Student Member, IEEE) was born in Hebei, China, in 1996. He received the B.E. degree in mechatronic engineering from Chang'an University, Xi'an, China, in 2019. He is currently working toward the Ph.D. degree in mechatronic engineering with the Changchun Institute of Optics, Fine Mechanics and Physics, Chinese Academy of Sciences, Changchun, China.

His research interests include electric machines and drives and high-precision machine control techniques.

Zongen Wei (Graduate Student Member, IEEE) was born in Shandong, China, in 1997. He received the B.E. degree in measurement and control technology and instrument from the Shandong University of Technology, Zibo, China, in 2020. He is currently working toward the Ph.D. degree in mechatronic engineering with the University of Chinese Academy of Sciences, Beijing, China, and the Changchun Institute of Optics, Fine Mechanics and Physics, Chinese Academy of Sciences, Changchun, China.

His research interests include ac motor drive and control design, model-predictive control, and digital control with DSP.

Haiyang Cao (Graduate Student Member, IEEE) was born in Shangdong, China, in 1997. He received the B.E. degree in mechanical design, manufacturing and automation from Northeast Petroleum University, Daqing, China, in 2020. He is currently working toward the Ph.D. degree in mechatronic engineering with the University of Chinese Academy of Sciences, Beijing, China, and the Changchun Institute of Optics, Fine Mechanics and Physics, Chinese Academy of Sciences, Changchun, China.

His main research interests include advanced control theories and applications on motor drive systems.